

## Article

# Slope Stability Analysis for a Large Hydropower Station in China

Dongbin Yin <sup>1</sup>, Huifen Liu <sup>2,\*</sup>, Jingwen Yan <sup>1</sup> and Jianqiang Wang <sup>3</sup><sup>1</sup> College of Engineering, Shantou University, Shantou 515063, China<sup>2</sup> School of Transportation, Civil Engineering and Architecture, Foshan University, Foshan 528231, China<sup>3</sup> Guangdong Wisdom Cloud Engineering Science and Technology Co., Ltd., Foshan 528200, China

\* Correspondence: liuhuifen99@163.com

**Abstract:** Hydropower plants (including the switching station) built in the middle and southern section of the north–south zone of China are always situated in complex geological settings of transition zones from strong to weak earthquakes with active faults. It is of great importance to carry out careful evaluation of the slope stability considering various loading scenarios to ensure safe operation of the power stations. By using the rigid body limit equilibrium method and the finite element method, the effects of long-term load and seismic load on slope stability for a large hydropower station were studied. The results show that the slope safety factors of the station meet the stability requirements when the slope is under long-term load and under the action of the Wenchuan and Lushan earthquake loads. The stability of the slope is guaranteed. However, the risk analysis of the slope stability under the action of the design earthquake load shows that the slope safety factor is less than the accidental working condition safety factor of 1.05. Under the action of a strong earthquake, the crumbling block gravel soil layer in the shallow natural slope slides and destabilizes, which is obviously beyond its protection capacity, and therefore, effective seismic defense measures should be developed to ensure the safety of the personnel and equipment operating in the power station and switching station.

**Keywords:** slope stability analysis; long-term load; earthquake loads; rigid body limit equilibrium method; finite element method



**Citation:** Yin, D.; Liu, H.; Yan, J.; Wang, J. Slope Stability Analysis for a Large Hydropower Station in China. *Sustainability* **2023**, *15*, 3561. <https://doi.org/10.3390/su15043561>

Academic Editors: Jiankun Huang, Yunqi Wang, Liqun Lyu and Jun Li

Received: 3 January 2023

Revised: 26 January 2023

Accepted: 9 February 2023

Published: 15 February 2023



**Copyright:** © 2023 by the authors. Licensee MDPI, Basel, Switzerland. This article is an open access article distributed under the terms and conditions of the Creative Commons Attribution (CC BY) license (<https://creativecommons.org/licenses/by/4.0/>).

## 1. Introduction

With the rapid development of China's economy, infrastructures such as those for hydropower stations, roads, bridges, and tunnels are under construction. Slopes are often encountered in the construction of infrastructure projects. The destabilization damage of slopes can cause serious human casualties and economic losses [1]. Therefore, it is of great importance to perform the stability analysis of slopes.

Numerous scholars have studied the stability of slopes, such as Fan [2] and Gao, et al. [3] who used rigid body limit equilibrium for three-dimensional soil slope stability studies; Zhao, et al. [4], Zhang [5], Guo, et al. [6], and Lin, et al. [7] conducted slope stability analysis based on the finite element method. Both methods have been well demonstrated in three-dimensional slope stability analysis under complex geological conditions and slope geometries. In addition, the strength reduction method is also widely used in slope stability analysis, such as the material parameter reduction method proposed by Wu, et al. [8], Han, et al. [9], the “reduced” strength envelope method proposed by Hammah, et al. [10], the graphical method [11,12] to calculate the minimum safety factor of slopes. Zhang, et al. [13] analyzed the seismic safety of a hydropower station slope by the strength reduction method. While there are many methods for slope stability analysis, this study was focused on the rigid body equilibrium and finite element methods.

As important factors that induces slope instability, the influences of earthquake and rainfall on slope stability have also attracted much research attention. For example, Liu, et al. [14] proposed evaluation of the stability of seismically acting slopes by using the minimum average safety factor. Qi, et al. [15] stated that slope instability under seismic load is caused by the action of a seismic inertia force, resulting in a rapid increase of excess pore water pressure and its cumulative effect. Wang, et al. [16] studied the slope stability under the coupled action of earthquake and rainfall by shaking table tests. Xu, et al. [17] analyzed the influence of seismic dynamic parameters and seismic dynamic responses on the slope. Ye, Tang, and others [18,19] agreed that rainfall infiltration causes changes in soil properties, which affect the stability of slopes. Lin, et al. [20] found that strong rainfall is likely to cause flow-slip damage and erosion of slopes, and low rainfall is likely to cause an increase of pore water pressure in the deep soil of slopes, thus triggering slope instability.

In this study, the slope stability of a large hydropower station in China (referred to as the Y hydropower station) was assessed. The slope of the Y hydropower plant (including the switching station) involves complex geological conditions as well as having a special geographic location. The project area of the station site is located in the middle and southern section of the north–south zone of China, on the transition zone from strong to weak earthquakes with active faults. Historically, earthquakes with high frequencies and magnitudes in that area have been reported, including the Wenchuan “5.12” earthquake in 2008 and the Lushan “4.20” earthquake in 2013. The seismic effect could pose serious safety issues to employees and the station equipment once the slope fails. It would cause huge economic loss. Therefore, it is of great significance to carry out further evaluation on the stability of the slope of the station to ensure safe operation of the power station [21,22].

Slopes in complex geological conditions, e.g., fractured rocks, veins, interfaces, near an active fault zone, are prone to fail due to various triggering factors, especially earthquake hazards [23–30]. Therefore, the stability of slopes should be carefully evaluated by considering different working scenarios, for example, long-term, transient, and accidental cases [21,22] with the utilization of different analysis methods. In this regard, this study aimed to re-assess the slope stability under long-term loads and the effects of the Wenchuan earthquake, Lushan earthquake, and a design earthquake through both the rigid body limit equilibrium method and finite element method. The most unfavorable sliding surface, safety factors, deformation damage mode, and deformation damage mechanism of the slope under earthquake and groundwater actions were investigated. The stability of the slope of the Y hydropower station was comprehensively evaluated, the trend of stability evaluation for the landslide body was predicted, and reasonable suggestions for slope reinforcement are provided. This study is of great significance to accurately grasp the operational condition of the slope of the Y hydropower station and ensure the long-term stability and safety of the slope.

## 2. Project Overview and Slope Monitoring Program

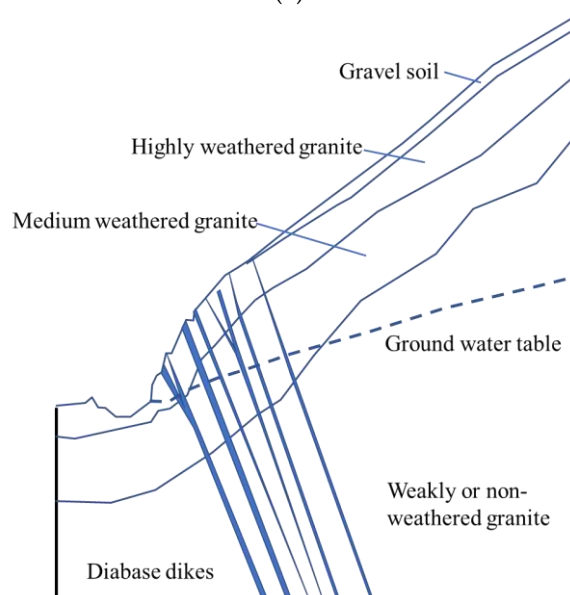
The Y hydropower station is located in a high mountain valley area in Sichuan Province, China. Since the river valley is very deep, both sides of the valley form steep slopes. The upstream and downstream of the river are cut by a gully, the station is situated on the right bank, upstream of the Y village. The ground elevation of the station area is about 1377 m, composing of rocky slopes below 1438 m elevation and a block gravel soil slope above 1438 m elevation. Figure 1a shows the overall view of the high slope of the Y hydropower station, while Figure 1b shows the geological profile of the slope.

The longitudinal axis of the plant is roughly parallel to the direction of the slope back edge, and the back slope of the switch station section intersects the back slope of the plant section at an angle of about  $41.5^\circ$ . The natural slope height is greater than 400 m, and the slope degree is between  $40^\circ$  and  $50^\circ$ . The maximum slope height after excavation is about 130 m, and two levels of transportation paths are set up at elevations 1410 m and 1438 m. The face of the excavated slope below the 1410 m transportation path is  $70\text{--}75^\circ$  from the horizontal, while the excavated slope between the two paths is  $55\text{--}65^\circ$ , and the slope above

1438 m path is about  $40^\circ$ . The entire slope is about 140 m long, and the slope face area comprises about 20,000 m<sup>2</sup>.



(a)



(b)

**Figure 1.** The high slope behind Y hydropower station: (a) full view; and (b) geological profile.

The geological conditions of the Y hydropower station slope are complex [31]. The surface of the slope is gravel soil, 5–10 m thick, and the residual slope gravel layer is about 2–5 m thick above an elevation of 1438 m to the slope of the opening line, with loose structure and local hollow cavities. The slope is basically composed of coarse-grained granite, interspersed with eight pyroclastic veins which form a nearly parallel arrangement and an oblique intersection with the center line of the plant at a later stage. There are three groups of fissures distributed inside the slope, and the slope is cut by pyroclastic veins and three groups of fissures, which make the slope rock mass inadequate with respect to stability conditions. The rocks are mainly weak and slightly weathered. During the construction of the station, local shallow rock collapse and sliding occurred many times along the slope fissures, the unfavorable structural surfaces, and the contact surfaces between the overburden and the bedrock.

The project area of the Y hydropower plant site is located in the middle and southern part of the north–south zone of China, on the transition zone from strong to weak

earthquakes with active faults. Historically, the frequency of earthquakes is high, and the magnitude is large. As of 2014, five strong earthquakes of magnitude 7 and higher, 13 earthquakes of magnitude 6–6.9, and 19 earthquakes of magnitude 5–5.9 had been recorded, and the station slopes experienced the 2008 Wenchuan “5.12” earthquake and the 2013 Lushan “4.20” earthquake, among others. Earthquakes can have a large impact on the stability of the slope of the Y hydropower plant.

In order to monitor the deformation, seepage, and stress–strain of the plant and the high slope surrounding rocks, verify the calculation results of the rock stability, and ensure safe operation, seven monitoring sections were set up in the plant and slopes, while two active inclination measurement tubes, IN1 and IN3, were installed on the high slopes at an elevation of 1446.0 m. An IN2 inclination measurement tube was installed on the high slope at an elevation of 1410.0 m to monitor the slope displacements. The monitoring of the slopes includes four items: internal displacement of the slope, anchor stress, anchor cable tension, and groundwater table. Figure 2 shows the measured groundwater table over time.

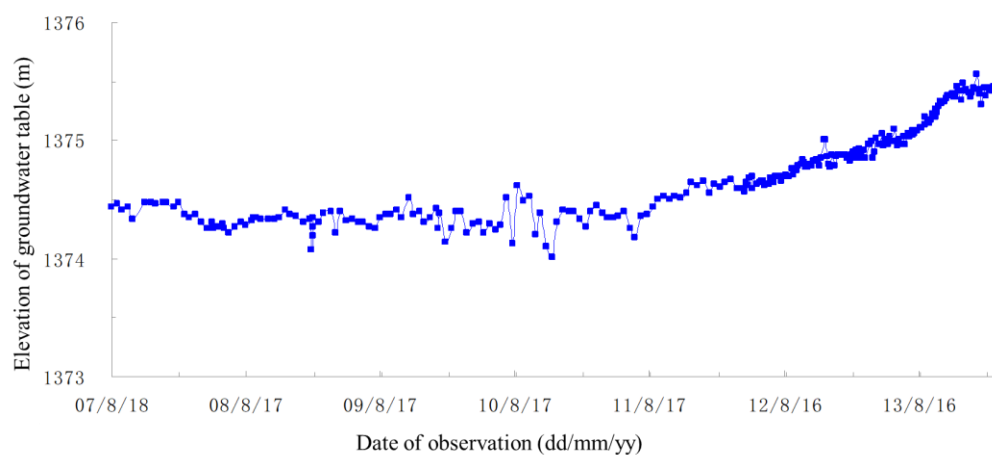


**Figure 2.** Measured groundwater table with time for the slopes.

### 3. Calculation Principle and Calculation Method

This study aimed to analyze the possible sliding surfaces in each sliding mode and determine the most dangerous sliders and their safety factors by the rigid body limit equilibrium method and the finite element numerical simulation method, mainly based on the fracture yield and the nature of the overlying soil, for the following two possible sliding modes.

Among them, sliding mode I is the part of the cover layer of the crumbling slope block soil layer, 1438 m elevation to the opening line (1503 m). The shallow surface of the crumbling slope block soil layer was not excavated above the opening line, the shear strength index is low, and there is the possibility of shallow sliding along the inside of the cover layer and sliding along the interface between the cover layer and the bedrock. Sliding mode II is a fractured rocky slope below 1438 m elevation of the plant slope, and the possible sliding mode is a composite sliding surface composed of two groups of fractured-steep dip and slow dip in the direction of the slope.

This section briefly introduces the rigid body limit equilibrium method, the finite element analysis method, and the calculation conditions considered in this study. Although when using either method it is possible to obtain stability calculation results of the slopes, this study used both for two reasons: First, this hydropower station is a mega project and its importance is ranked very high; thus, the stability assessment should be assessed from different angles, which is treated as another layer of safety. Second, it is desirable to cross check the validity of these two methods for this project, which will be very helpful for future assessment and slope management.

### 3.1. Rigid Body Limit Equilibrium Method

The rigid body limit equilibrium method takes the Mohr–Coulomb damage criterion as the theoretical basis and establishes the equilibrium equation to solve the safety factor of the slope. The rigid body limit equilibrium method assumes that the geotechnical body is a rigid body and considers the damage of the slope as a plane strain problem, and expresses the safety factor of the slope with the ratio of the shear strength along the sliding surface and the strength exerted by the geotechnical body to maintain equilibrium when the slope reaches a stable state.

One of the more common methods available is the strip splitting method, in which the sliders are vertically strip split, as shown in Figure 3. The safety factor of the slope is obtained by equilibrium analysis of each strip.

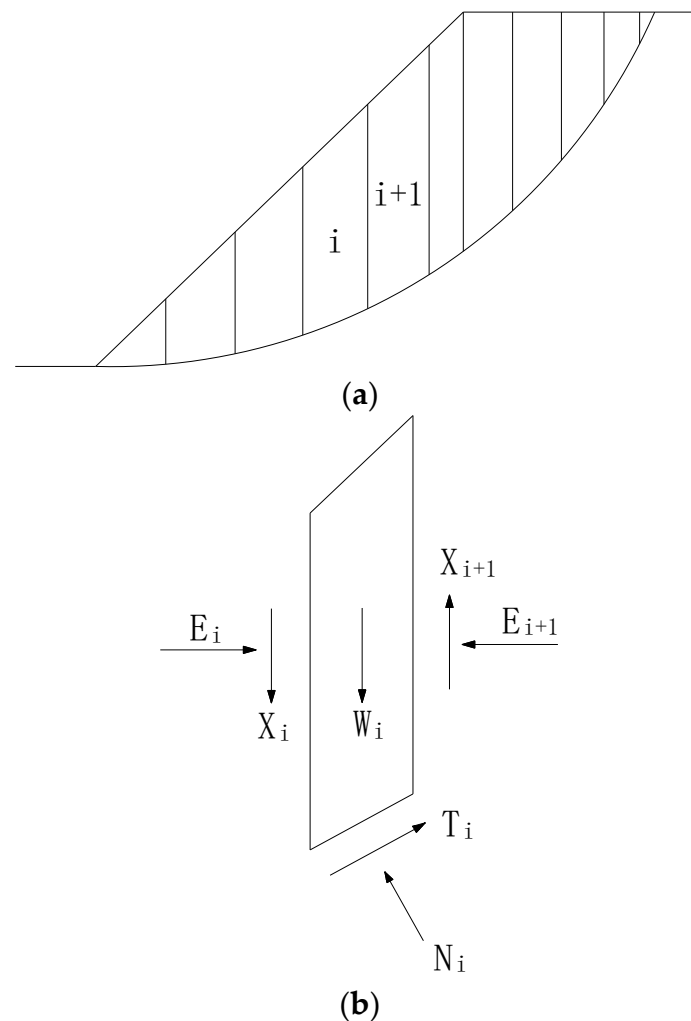


**Figure 3.** Schematic illustration of the strip splitting method. (a) Schematic diagram of the strip splitting method. (b) Schematic diagram of force balance in a strip.

According to the different assumptions of the rigid body limit equilibrium method, it can be divided into various calculation methods, such as Bishop method, Janbu method, Morgenstern–Price method, Spencer method, Sarma method, etc. The Design Specification for Slopes in Water and Hydropower Projects stipulates the following [32]: “For soil slopes or rocky slopes with fractured and bulk structures, when the sliding surface is circular, it is appropriate to use the simplified Bishop method and the Morganston–Price method; for the calculation of anti-slip stability, when the sliding surface is non-circular, it is appropriate to use the Morganston–Price method and the unbalanced thrust transfer method for the calculation of anti-slip stability”.

Therefore, in this study, the simplified Bishop method was used in calculating the sliding of the overburden slopes along the shallow or interface with the bedrock (i.e., sliding mode I), and the Morganstein–Price method was used in calculating the safety factor of a composite sliding surface composed of downhill fissures (i.e., sliding mode II) to determine the slope stability.

### 3.2. Finite Element Analysis Method

Using the results of the finite element method, the factor of safety for slip resistance along the sliding surface is calculated as:

$$F_s = \frac{\int (c + \sigma_n \tan \phi) dl}{\int \tau_m dl} \quad (1)$$

where the slip resistance is based on the Mohr–Coulomb shear strength criterion.  $\sigma_n$  is the normal stress at the bottom center point of the soil strip, and  $\tau_m$  is the tangential slip shear stress at the bottom center point of the soil strip.

Factor of safety for stability along the slip crack surface is as follows:

$$F_s = \frac{\sum (c_i + (\sigma_n - u_i) \tan \phi_i) l_i}{\sum \tau_m l_i} \quad (2)$$

where,  $c_i$  is the effective cohesion at the bottom of the soil strip;  $\phi_i$  is the angle of internal friction;  $l_i$  is the length of the bottom of the soil strip;  $u_i$  is the pore water pressure at the bottom of the soil strip.

In this study, the ideal elastic-plastic constitutive model was used for the materials of slope in the stress-deformation calculation. The implicit unit method was used to simulate anchor bolts in the stress calculation, the two-node bar element to simulate anchor cables, and the space shell unit to simulate the surface shotcrete support measures. The frame lattice beams were simulated with the beam element.

The radiation damping effect of the foundation was considered in the seismic dynamic analysis of the slope. A finite calculation area was cut out from the semi-infinite foundation medium, and an artificial boundary established on the cut boundary to simulate the radiation damping of the continuous medium, i.e., spring dampers were placed on the boundary to ensure that the scattered waves passed through the artificial boundary from inside the finite calculation area without reflection.

### 3.3. Calculated Load and Working Conditions

The main calculated loads considered in this study are self-weight, groundwater hydrostatic pressure, ground stress, support reinforcement force, and earthquake load. The calculated working conditions include long-term and accidental working conditions, and their combinations. The loading scenarios are as follows.

Scenario 1. Long-term working condition—Basic combination: initial stress field + excavation unloading + geotechnical body self-weight + support reinforcement force + groundwater hydrostatic pressure;

Scenario 2. Accidental working conditions—Scenario 1 + Wenchuan earthquake: initial stress field + excavation unloading + geotechnical body self-weight + Wenchuan earthquake measured value + support reinforcement force + groundwater hydrostatic pressure;

Scenario 3. Accidental working conditions—Scenario 1 + Lushan earthquake: initial stress field + excavation unloading + geotechnical body self-weight + Lushan earthquake measured value + support reinforcement force + groundwater hydrostatic pressure;

Scenario 4. Accidental working conditions—Scenario 1 + Normative spectrum artificial wave: initial stress field + excavation unloading + geotechnical body self-weight + artificial wave seismic + support reinforcement force + groundwater hydrostatic pressure;

Scenario 5. Accidental working conditions—Scenario 1 + Wenchuan earthquake amplification to design ground shaking seismic waves: initial stress field + excavation unloading

+ geotechnical body self-weight + Wenchuan earthquake amplification to design ground shaking seismic wave + support reinforcement force + groundwater hydrostatic pressure;

Scenario 6. Accidental working conditions—Scenario 1 + Lushan earthquake amplification to design ground shaking seismic wave: initial stress field + excavation unloading + geotechnical body self-weight + Lushan earthquake amplification to design ground shaking seismic wave + support reinforcement force + groundwater hydrostatic pressure.

#### 4. Results of Slope Stability Analysis

The high slope behind the plant of the Y hydropower station is proposed as the slope of the Class IIA hub engineering area. According to the specification Design specification for slope of hydropower and water conservancy project [33], when the lower limit solution in the limit balance method is used, the factor of safety under the corresponding lasting condition should not be less than 1.15–1.25; the factor of safety under the accidental condition should not be less than 1.05. The factor of safety of the engineering design in this study was taken as follows. The factor of safety in the long-term working condition should not be less than 1.20; the factor of safety in the accidental working condition should not be less than 1.05.

The process line of the inter-annual change of slope displacement monitoring shows that the slope displacement is basically stable and convergent, and the maximum displacement value of the plant slope is about 20 mm during the monitoring period. The slope displacement distribution map shows that the slope displacement in the part above 1441 m elevation is obviously larger than the lower slope displacement.

The process line of the water level of the plant slope seepage pressure meter and pressure measuring tube show that the groundwater level changes with the season, the water level is higher in the summer rainy season, the change of groundwater level deep in the slope body is larger, and the change of groundwater level near the surface of the slope body is reduced. It indicates that the rock body near the slope body is highly permeable and has good drainage performance. The low groundwater level in the slope body of the side slope is beneficial to the stability of the side slope.

This section further studies the slope stability under long-term operation conditions and the effects of the Wenchuan earthquake, the Lushan earthquake and a design earthquake on the slope stability through the rigid body limit equilibrium method and the finite element method, respectively, and analyzes the most unfavorable sliding surface and the corresponding factor of safety of the slope under accidental working conditions such as earthquake and groundwater action.

It is worth noting that the slope stress, deformation conditions, and monitoring data before and after the earthquake under different working conditions were analyzed in this study. For brevity, only the most dangerous slip surface of the slope under different working conditions and the corresponding factor of safety are discussed in this paper. The parameters that were used to carry out the stability analyses are summarized in Table 1.

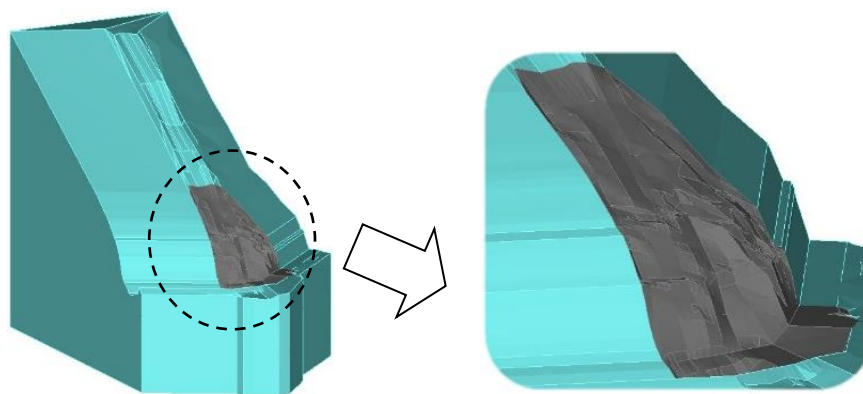
##### 4.1. Stability Analysis under Long-Term Operating Working Conditions

The Design specification for the slope of the hydropower and water conservancy project [33] requires that the calculation range of the stress–strain analysis should be determined according to the distribution of the self-weight stress field of the slope. The natural slope height of the slope behind the plant of the Y hydropower station is larger than 400 m, and the slope degree is 40–50°. The calculation range selected for this study was 200 m below the bottom of the slope in the direction of the slope height, 200 m above the opening line at the top of the slope. Vertical side slopes are taken outside the slope to the symmetrical position of the river valley, and 300–500 m towards the complete rock in the slope, including the complete plant section and the switch station section along the slope. The three-dimensional finite element calculation model of the slope is shown in Figure 4.

**Table 1.** Materials parameters of hydropower station Y.

Material	Soil/Rock Parameter						Structural Surface Parameter	
	Elastic Modulus, $E$ (GPa)	Poisson's Ratio, $\mu$	Tensile Strength, $R_m$ (MPa)	Unit Weight, $\gamma$ (kN/m <sup>3</sup> )	Cohesion, $c$ (kPa)	Internal Friction Angle, $\varphi$ (°)	Cohesion, $c$ (kPa)	Internal Friction Angle, $\varphi$ (°)
Medium to coarse grained granite, strongly weathered, strong unloading zone	1.0–2.0	0.30	1.2–1.5	26.1	50–100	26–29	75	35
Medium to coarse grained granite, weakly weathered, weakly unloading zone	2.5–4.0	0.27	2.5–3.0	26.4	400–600	35–37	90	35
Medium to coarse grained granite, slightly weathered, intact rock	5.5–8.0	0.25	3.5–4.5	26.5	800–1000	40–45	100	35
Overburden layer	0.1	0.35	0.5–0.8	11.5–20	27	28	15	25
Fault and vein fracture zone	0.8	0.30	N/A	26.1	70	28	N/A	N/A
Rock chip interspersed mud structure surface	N/A	N/A	N/A	N/A	N/A	N/A	20–30	21–24
Anchor bolt	210	0.30	N/A	7800	N/A	N/A	N/A	N/A
Anchor cable	210	0.30	N/A	7800	N/A	N/A	N/A	N/A
Shotcrete (C20, surface thickness 12 cm)	25.5	0.167	N/A	2400	N/A	N/A	N/A	N/A
Frame beam (C25)	28	0.167	N/A	2400	N/A	N/A	N/A	N/A
Anchor cable foundation beam (C25)	28	0.167	N/A	2400	N/A	N/A	N/A	N/A

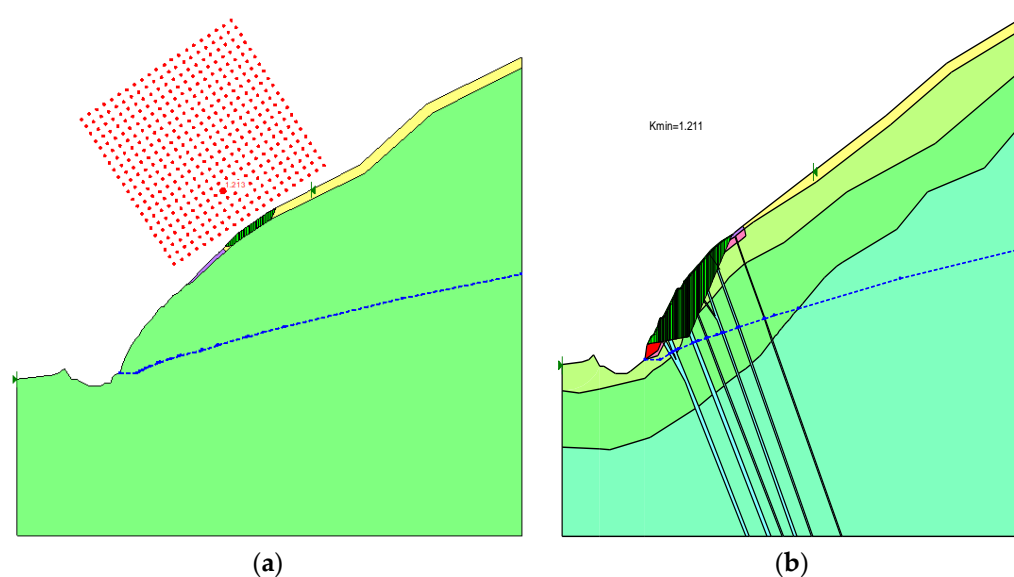
Note: N/A = Not Applicable.

**Figure 4.** The three-dimensional finite element calculation model of the slope.

Based on the analysis of slope stress, deformation, and distribution of the plastic zone by the elastic-plastic finite element method, a total of eight sections of plant and switching station were selected for calculation, namely, plant 0+000, plant 0+014, plant 0+028, plant 0+038, plant 0+051, switching 0+031, switching 0+043, switching 0+062 as the calculation profiles. The stability safety of the slope under long-term operating working conditions was analyzed by the rigid body limit equilibrium method and finite element method, including the search of the most dangerous sliding surface under two sliding modes and the calculation of the factor of safety of the most dangerous sliding surface. Table 2 shows the factor of safety of the most dangerous sliding surface in each section; Figure 5 shows the most dangerous sliding surface corresponding to the minimum factor of safety for the rigid body limit equilibrium method in different sliding modes.

**Table 2.** Factor of safety of the most dangerous sliding surface for long-term working conditions.

Section	Factor of Safety of the Most Dangerous Sliding Surface			
	Sliding Mode I		Sliding Mode II	
	Rigid Body Limit Equilibrium Method	Finite Element Method	Rigid Body Limit Equilibrium Method	Finite Element Method
Plant 0+000	1.264	1.712	1.266	2.375
Plant 0+014	1.388	1.786	1.211	2.984
Plant 0+028	1.310	1.823	2.116	2.831
Plant 0+038	1.213	1.958	1.409	3.086
Plant 0+051	1.334	1.326	1.392	2.534
Switching 0+031	1.624	2.057	1.234	1.692
Switching 0+043	1.234	1.873	1.271	1.562
Switching 0+062	1.326	1.365	1.227	1.593

**Figure 5.** Minimum factor of safety of slope by rigid body limit method under different sliding modes. (a) Sliding mode I of the slope in the plant 0+038 section. (b) Sliding mode II of the slope in the plant 0+014 section.

From Table 2, the minimum factor of safety under sliding mode I, calculated by the rigid-body limit equilibrium method, is 1.213, which appears in the plant 0+038 section; the minimum safety factor under sliding mode II calculated by the rigid-body limit equilibrium method is 1.211, which appears in the plant 0+014 section. The minimum sliding surface appears in the plant section.

The finite element method calculates the minimum factor of safety as 1.365 for sliding mode I, which appears in the switching 0+062 section; the finite element method calculates the minimum factor of safety as 1.562 for sliding mode II, which appears in the switching 0+043 section. The minimum safety factor appears in the switching station section.

Overall, the minimum safety factor of the rigid body limit equilibrium method is 1.211 and the minimum safety factor of the finite element method is 1.365, both of which meet the requirement of the minimum design factor of safety of not less than 1.20 under long-term working conditions.

In general, regarding the analyses of two failure modes, i.e., mode I and II, mode I is for shallow slope failure of the surface soil layer, mode II is for deep slope failure of the fractured rock, as shown in Figure 5. The failure surface of mode I (above Elevation 1438) typically occurs along the interface between the soil layer and the bedrock. This interface is subjected to a stronger weathering process and is easily influenced by environmental factors such as rainfall, earthquake, fluctuation of ground water, vibration from human

activity, etc. Whereas for mode II (below Elevation 1438), although the bedrock has fissures, the failure surface must cut through deeply in order that the potential sliding rock mass slides. In addition, rock anchors were applied to stabilize the rock mass, which greatly reduced the possibility of occurrence of mode II. Therefore, in this project mode II is more stable than mode I.

#### 4.2. Stability Analysis under Accidental Working Conditions

##### 4.2.1. Stability Analysis under the Effect of the Wenchuan and Lushan Earthquakes

Before analyzing the stability of slopes under seismic loading, the changes of each monitoring value of the slopes before and after the Wenchuan and Lushan earthquakes were first analyzed. For the brevity of the paper, the specific monitoring analysis is not presented in detail in this study.

In general, the measured values of each point of slope monitoring before and after the Wenchuan and Lushan earthquakes did not change much. The maximum change in displacement before and after the Wenchuan earthquake is 0.2–3.23 mm, and the maximum change is 3.23 mm. The maximum change in the effective measured value of the anchor stress gauge was 1.12 MPa; the change in anchor cable force gauge was 54.92–18.85 kN, all of which show a decrease in anchor cable stress, while the maximum decrease was 54.92 kN. The seepage pressure meter, pressure tube water level change was 1.78–0.05 m, all showing a water level decline, while the maximum water level decline was 1.78 m.

The displacement change value before and after the Lushan earthquake was 2.08–0.3 mm, the maximum change value was 0.3 mm; the maximum change value of the anchor effective measurement value was 0.57 MPa; the anchor cable dynamometer change value was 385.57–21.7 kN, the decrease maximum value was 385.57 kN, the increase maximum value was 21.24 kN; the seepage pressure meter, the pressure measuring tube water level change was 0.86–0.04 m, all show a decline, with a maximum decline of 0.86 m.

In carrying out the stability of slopes under seismic loading, eight sections consistent with the previous section were selected as the calculation section, and the dynamic stability of slopes under the Wenchuan and Lushan earthquake conditions was analyzed using the finite element time course method. The time course curves of the dynamic stability factor of safety of the most dangerous sliding surfaces of the two sliding modes under dynamic loading were obtained. Table 3 shows the factor of safety of the most dangerous sliding surface under the Wenchuan and Lushan earthquake conditions. Figure 6 shows the time course curves of the most dangerous sliding surface under different sliding modes for the Wenchuan earthquake condition; Figure 7 shows the time course curves of the most dangerous sliding surface under different sliding modes for the Lushan earthquake condition.

**Table 3.** Factor of safety of the most dangerous sliding surface for Wenchuan and Lushan earthquake working conditions.

Section	Sliding Mode I					Sliding Mode II				
	Minimum Factor of Safety			Decrease in Percentage		Minimum Factor of Safety			Decrease in Percentage	
	Long-Term Load	Wenchuan	Lushan	Wenchuan	Lushan	Long-Term Load	Wenchuan	Lushan	Wenchuan	Lushan
Plant 0+000	1.712	1.472	1.553	14.02	9.29	2.375	2.204	2.216	7.2	6.69
Plant 0+014	1.786	1.501	1.606	15.96	10.08	2.984	2.638	2.797	11.60	6.27
Plant 0+028	1.823	1.498	1.576	17.83	13.54	2.831	2.608	2.706	7.88	4.42
Plant 0+038	1.958	1.574	1.695	19.61	13.43	3.086	2.935	2.973	4.89	3.66
Plant 0+051	1.326	1.091	1.161	17.72	12.44	2.534	2.391	2.43	5.64	4.10
Switching 0+031	2.057	1.683	1.806	18.18	12.20	1.692	1.51	1.489	10.76	11.99
Switching 0+043	1.873	1.635	1.726	12.71	7.85	1.562	1.437	1.514	8.00	3.07
Switching 0+062	1.365	1.181	1.252	13.48	8.28	1.593	1.311	1.354	17.70	15.00

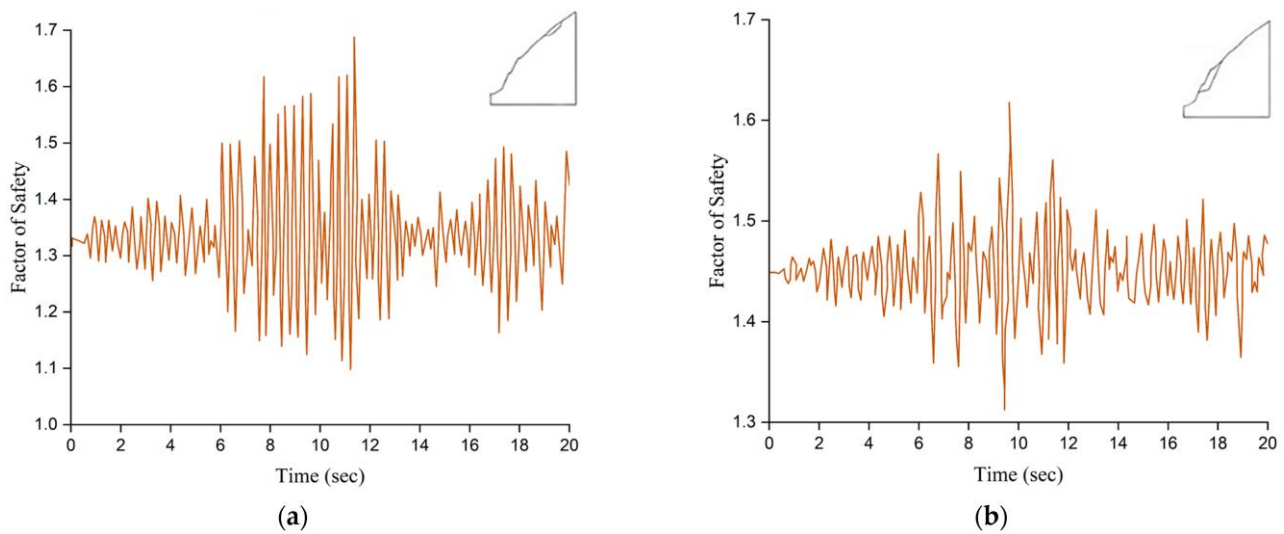


**Figure 6.** Time course curves of factor of safety of the most dangerous sliding surfaces under different sliding modes in Wenchuan earthquake. (a) Sliding mode I in the plant 0+051 section. (b) Sliding mode II in the switching 0+062 section.

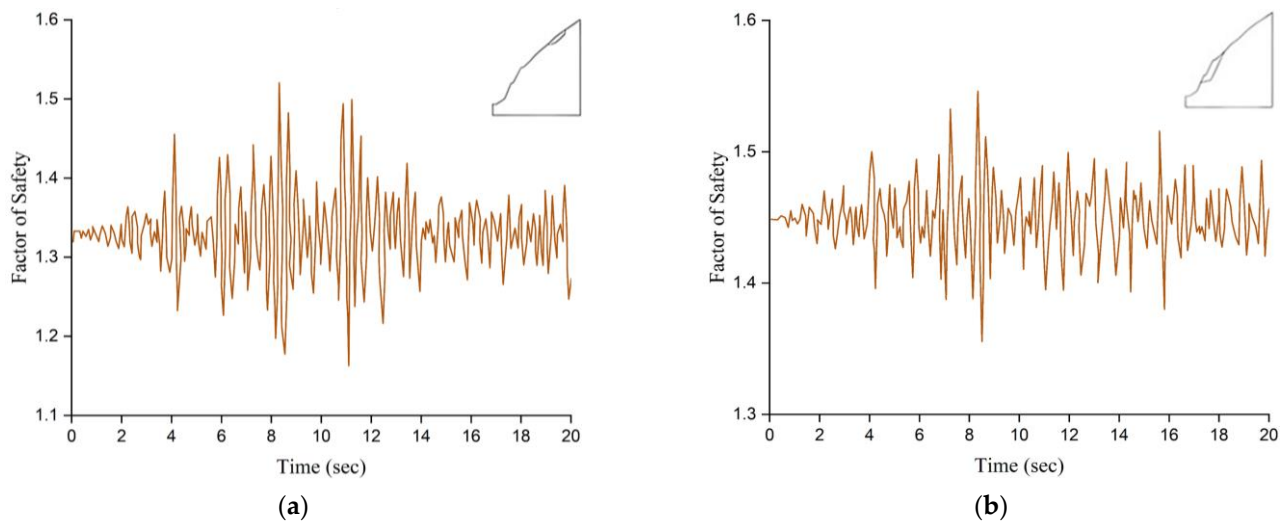


**Figure 7.** Time course curves of factor of safety of the most dangerous sliding surfaces under different sliding modes in Lushan earthquake. (a) Sliding mode I in the plant 0+051 section. (b) Sliding mode II in the switching 0+062 section.

Under the Wenchuan earthquake load, the sliding mode I slope stability factor of safety decreased by 12.71–19.61% and the sliding mode II decreased by 4.89–17.70% compared with the static long-term operating working conditions. The minimum value of factor of safety of the sliding mode I was 1.091, which appears in the 0+051 section of the plant; the minimum value of factor of safety of sliding mode II was 1.311, which appears in the 0+062 section of the switching station. Under the earthquake load of Lushan, the factor of safety of sliding mode I decreased by 7.85–13.54% and sliding mode II decreased by 3.07–15.00% compared with the static long-term operating working conditions. The minimum value of the sliding mode I factor of safety under the Lushan earthquake load was 1.161, which occurred in the switching 0+051 section of the plant, and the minimum value of the sliding mode II factor of safety was 1.354, which occurred in the 0+062 section of the switching station.

Overall, the minimum stability factor of safety for each section under the Wenchuan and Lushan earthquake loads meets the requirement of the factor of safety control standard of 1.05 under accidental working conditions. Since the source is far from the plant

site and the acceleration peak is small, the Wenchuan and Lushan earthquakes did not cause significant adverse effects on the overall stability of the high side slopes of the Y hydropower plant.

#### 4.2.2. Stability Analysis under Design Earthquake

From the accidental working conditions 3, it can be seen that there were three load combinations of design earthquakes considered in this study. They are the normative spectrum artificial wave, Wenchuan earthquake amplification to design ground shaking seismic waves, and Lushan earthquake amplification to design ground shaking seismic waves with basic combination, respectively. According to [34] at least two measured acceleration records and one artificially generated simulated seismic acceleration time course with the design response spectrum as the target spectrum should be selected when the seismic effect is calculated by the time course analysis method.

In this study, the canonical standard response spectrum was selected as the target spectrum to generate artificial seismic waves. The artificial wave was generated with an iterative error of 5%, where the characteristic period  $T_g$  was 0.2 s according to the bedrock site, the representative value of the maximum value of the response spectrum  $\beta_{max}$  was 2.25, the representative value of the design seismic acceleration was 0.2 g, and the peak vertical acceleration was taken as 2/3 of the peak horizontal acceleration, thus the seismic acceleration process line was obtained in 20 s. The normative spectrum artificial wave acceleration time curve is shown in Figure 8.

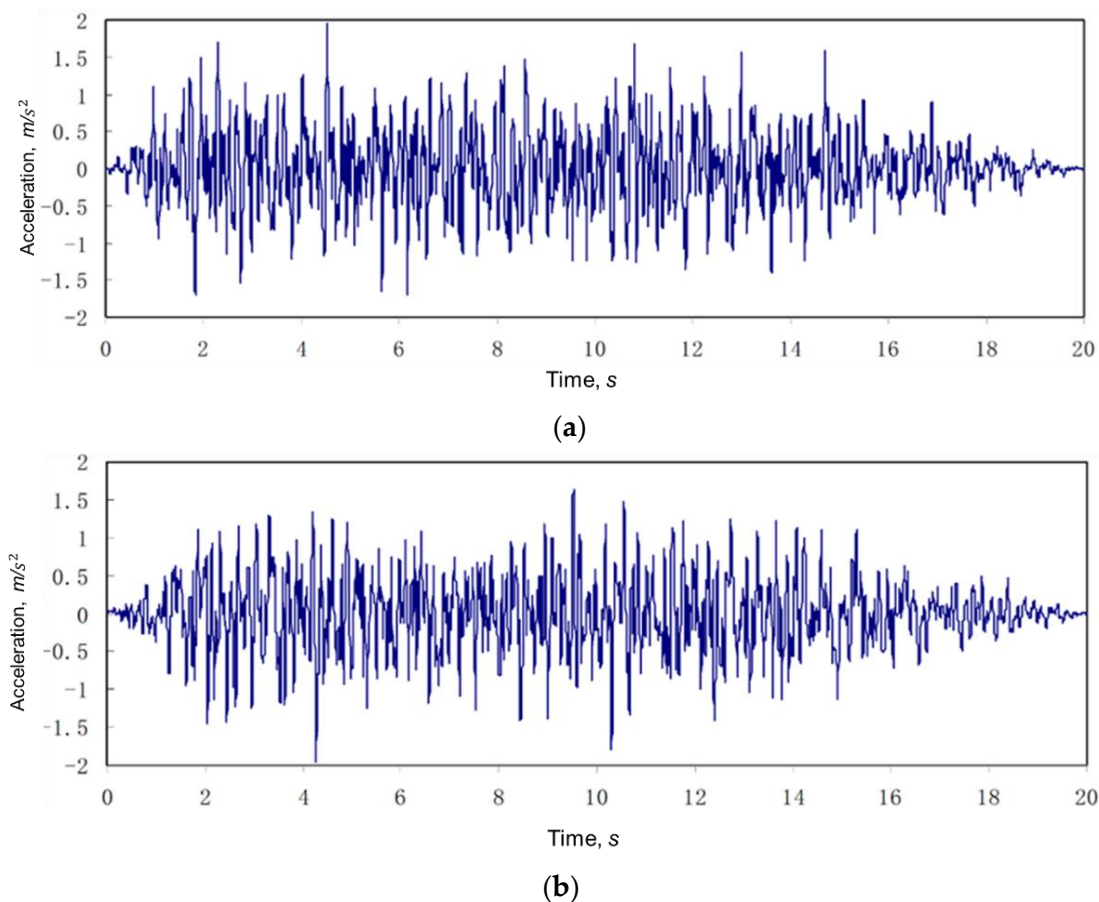
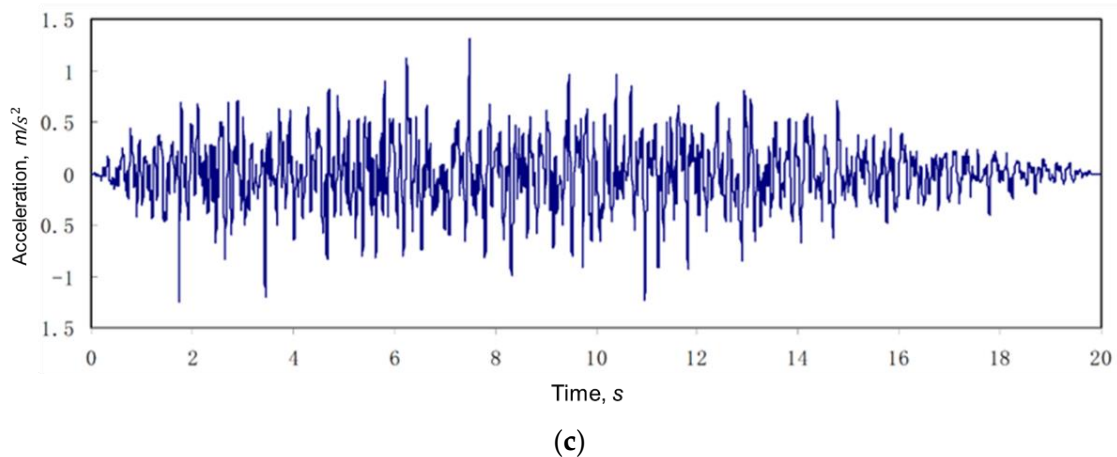
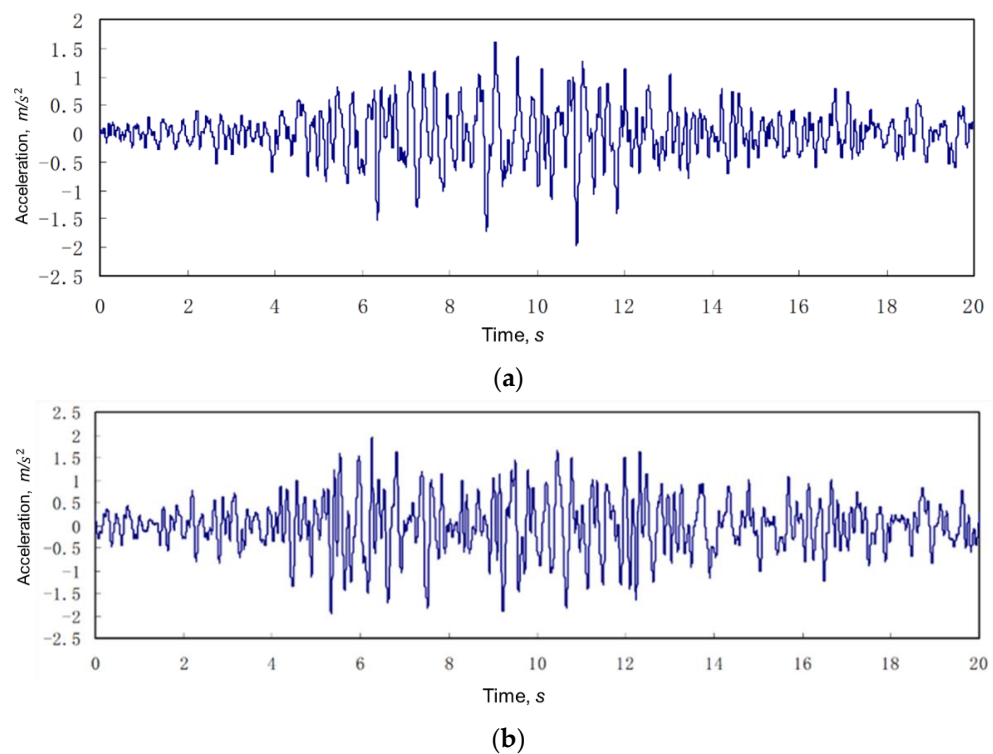


Figure 8. Cont.



**Figure 8.** Normative spectrum artificial seismic wave acceleration time curves. (a) Vertical slope orientation. (b) Along the side slope. (c) Vertical direction.

For the selection of the measured seismic waves, the Y hydropower station was the fourth stage of the planned terrace development in Nanya River Basin, while the Y hydropower station is the sixth stage of the planned terrace development in the Nanya River Basin and the regional geological structure is close. The measured seismic wave calculation was selected from the seismic monitoring records of the Y hydropower station, which was enlarged to the design intensity, i.e., the peak horizontal acceleration was enlarged to the peak design seismic acceleration of 0.2 g, and the peak vertical acceleration enlarged to 0.13 g. The acceleration time curves of the Wenchuan earthquake and Lushan earthquake enlarged to the design seismic intensity are shown in Figures 9 and 10. Figure 11 shows the frequency contents of these three earthquakes.



**Figure 9.** Cont.

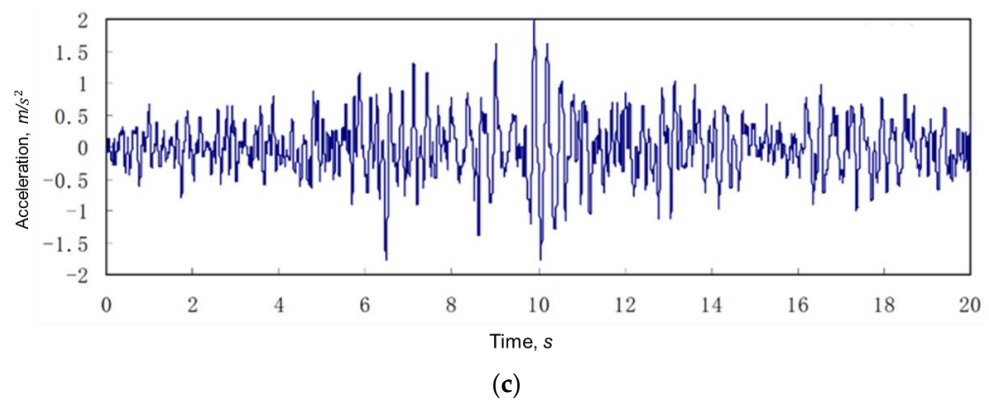


**Figure 9.** Wenchuan earthquake amplification to 0.2 g seismic wave acceleration time curve. (a) Vertical slope orientation. (b) Along the side slope. (c) Vertical direction.

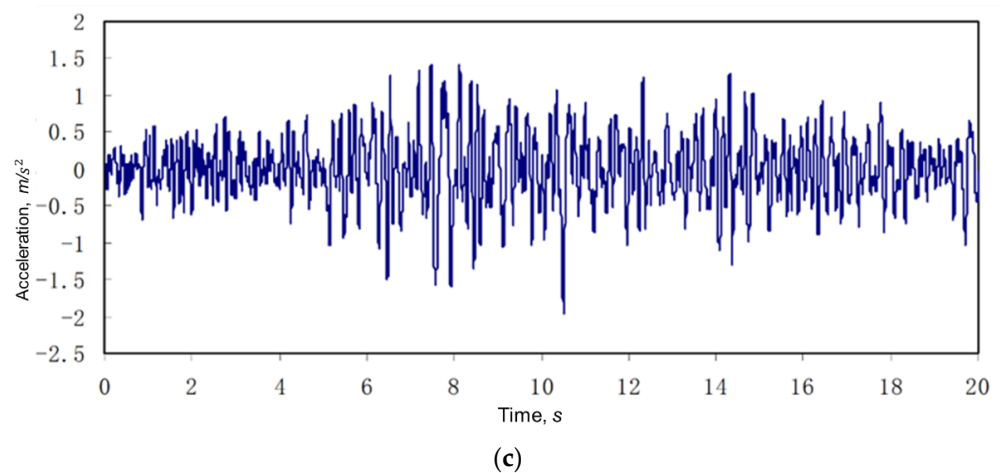
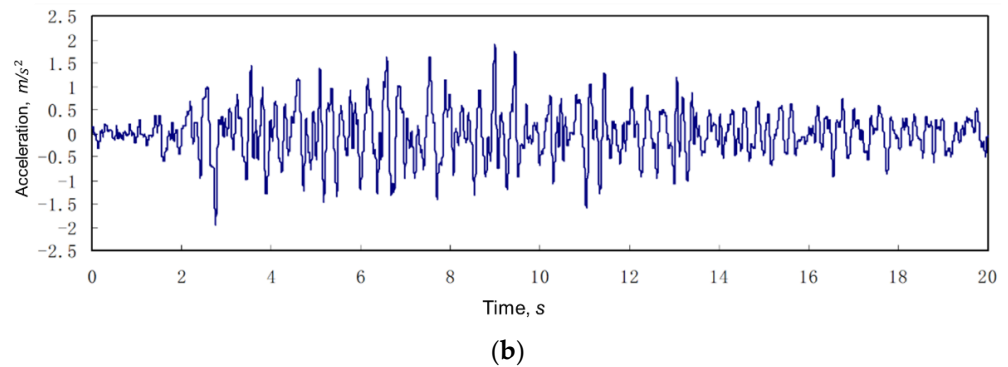
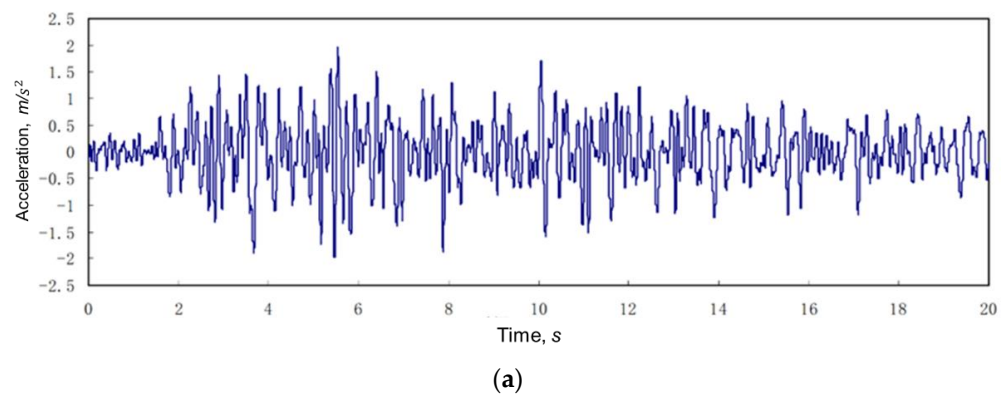


**Figure 10.** Lushan earthquake amplification to 0.2 g seismic wave acceleration time curve. (a) Vertical slope orientation. (b) Along the side slope. (c) Vertical direction.

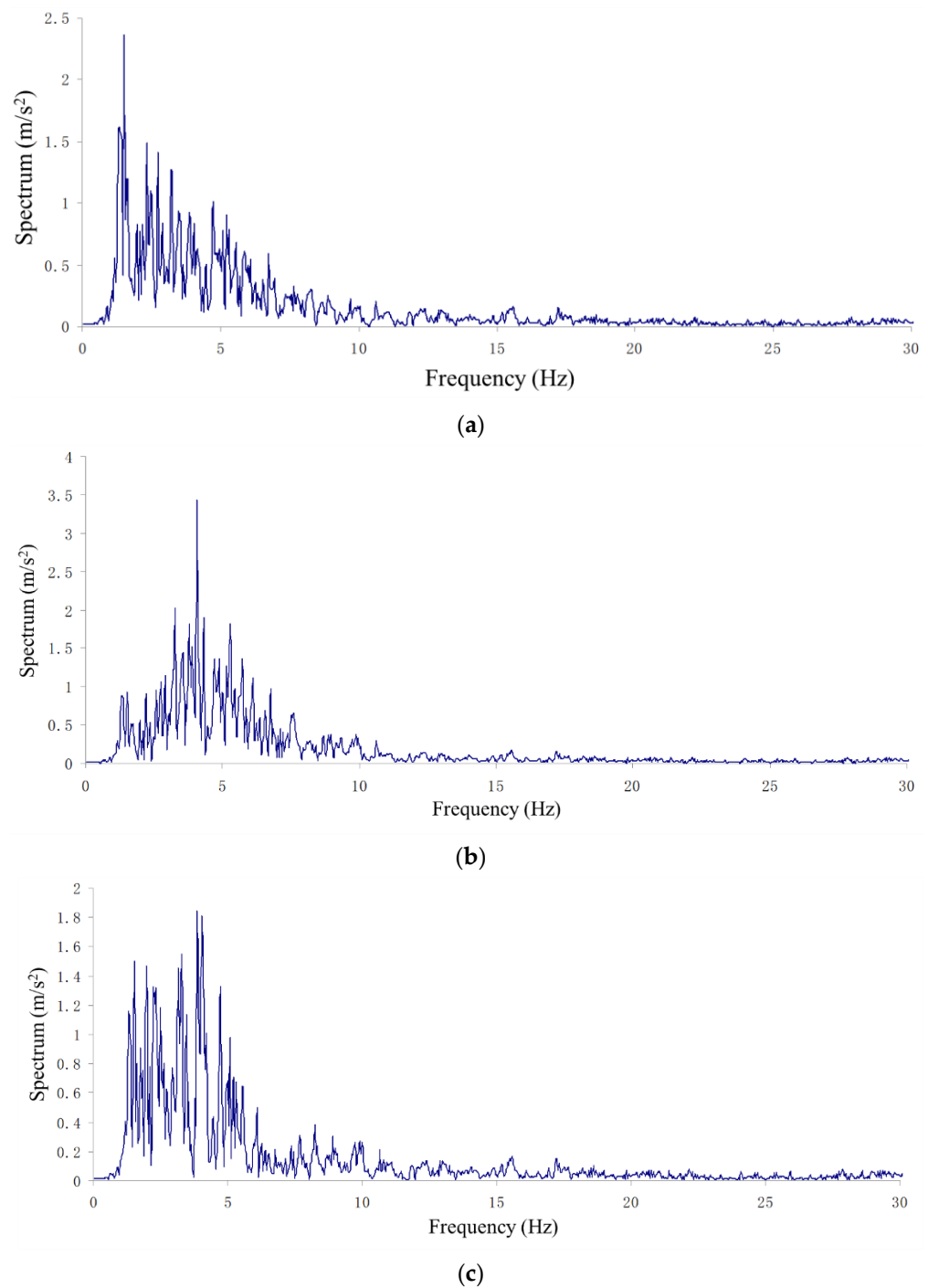


**Figure 11.** Frequency contents of the normative spectrum artificial seismic wave, Wenchuan earthquake, and Lushan earthquake. (a) Normative spectrum seismic wave. (b) Wenchuan earthquake. (c) Lushan earthquake.

In carrying out the slope stability under seismic loading, eight sections consistent with the previous section were selected as the calculation section, and the dynamic stability of the slope under the design seismic was analyzed by applying the finite element time course method to calculate the time course change curve of the dynamic stability factor of safety of the most dangerous sliding surface for the two sliding modes. Figure 12 illustrates the analysis outcomes of displacement, acceleration, and principle stresses of the hydropower station slope taking section plant 0+038 as an example. The first five modal shapes and the features for the same slope section are shown in Figures 13 and 14 and Table 4, respectively.

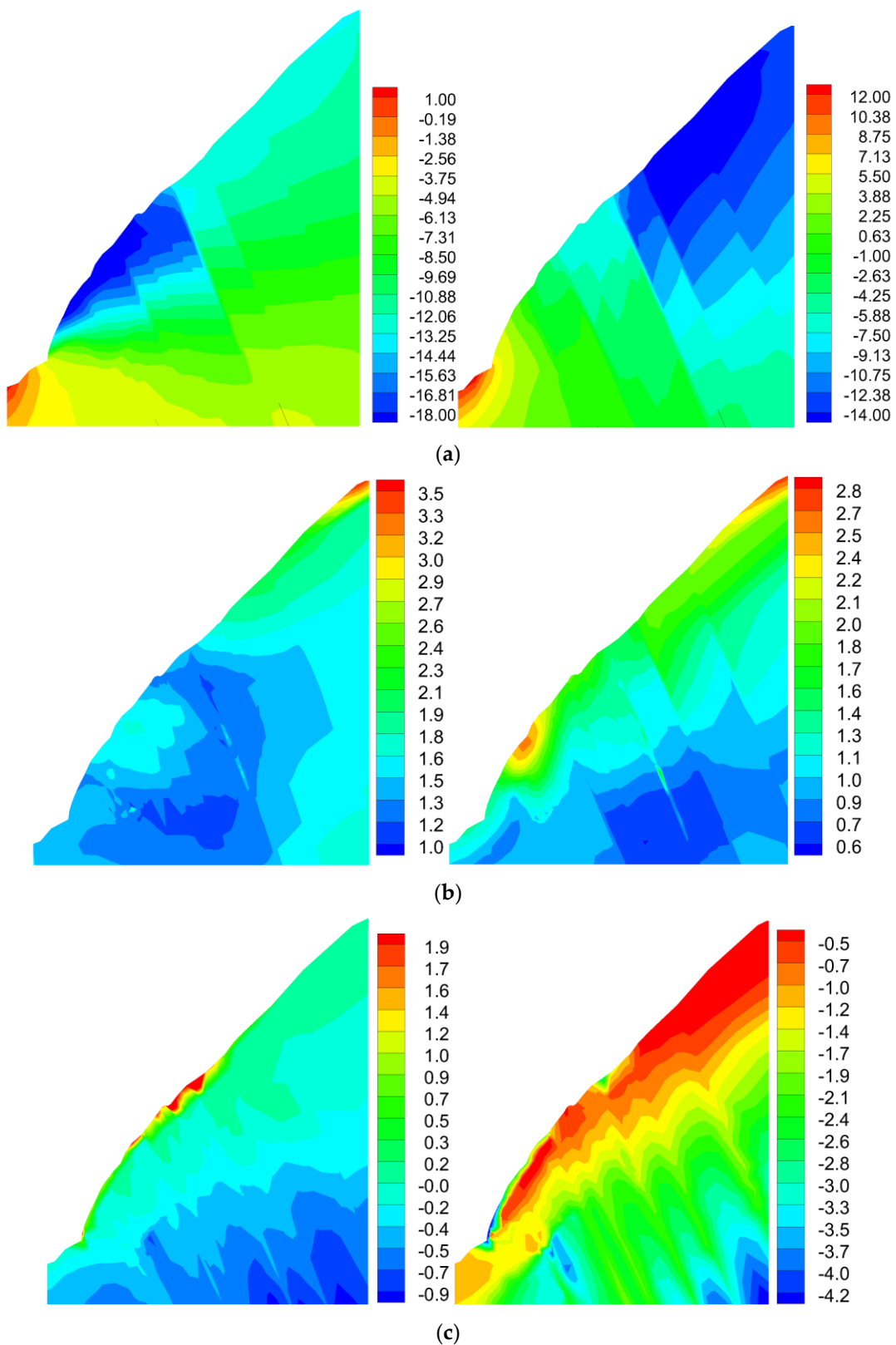


**Figure 12.** FEM analysis results of maximum displacement, acceleration and principle stresses for the hydropower station slope using section plant 0+038 as example. (a) Maximum displacement (unit: mm; left figure for horizontal, right figure for vertical). (b) Acceleration (unit:  $m/s^2$ ; left figure for horizontal, right figure for vertical). (c) Principle stresses (unit: MPa; left figure for the first, right figure for the third).

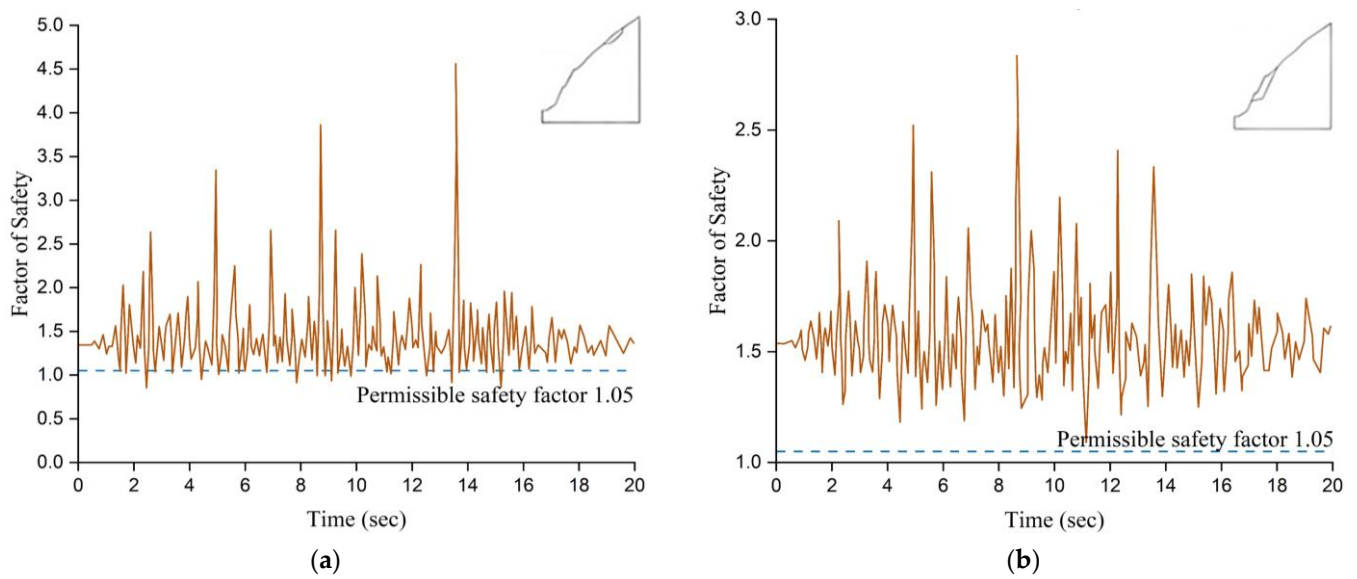


**Figure 13.** Time course curves of the most dangerous slip surface safety coefficients for the switching 0+062 section in different sliding modes under the normative spectrum artificial seismic wave. (a) Sliding mode I. (b) Sliding mode II.

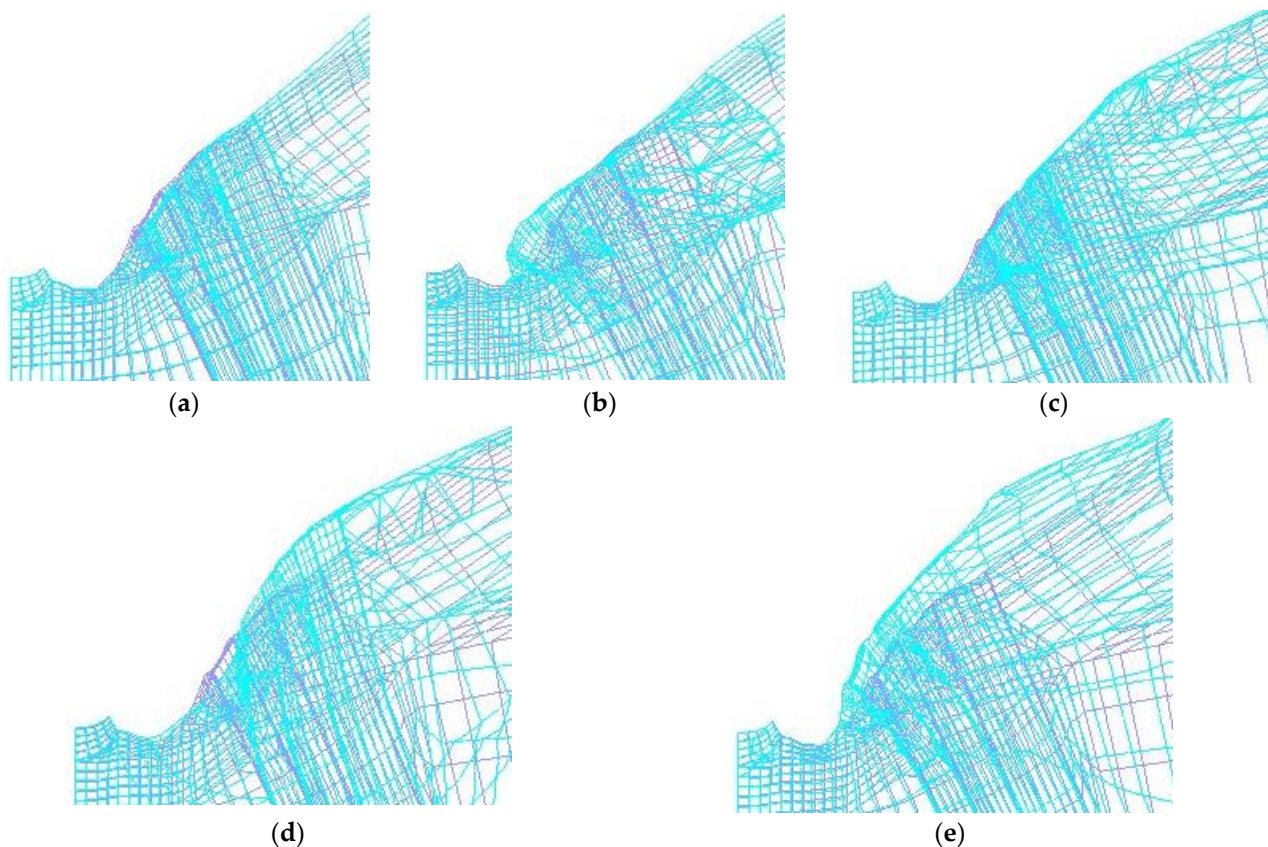


**Figure 14.** Modal shapes for the first five orders using Plant 0+038 slope section as example under the design earthquake load. (a) First-order modal shape. (b) Second-order modal shape. (c) Third-order modal shape. (d) Fourth-order modal shape. (e) Fifth-order modal shape.

**Table 4.** Vibration features and the first five modal shapes of the slope section of Plant 0+038.

Mode	Frequency of Self-Vibration (rad/s)	Frequency (HZ)	Period (s)	Modal Shape
1	6.899	1.098	0.911	Mainly vertical vibration with larger magnitude near the top
2	8.470	1.348	0.742	Mainly horizontal vibration with larger magnitude near the bottom
3	9.136	1.454	0.688	Horizontal torsion with larger magnitude near the top
4	9.808	1.561	0.641	Complex spatial vibration with larger horizontal torsion in the middle
5	10.204	1.624	0.616	Horizontal torsion with larger magnitude near the top

Table 5 shows the factor of safety of the most dangerous sliding surface under the design seismic condition. Figure 10 shows the time course curves of the factor of safety of the most dangerous sliding surface corresponding to the minimum factor of safety under different sliding modes of the normative spectrum artificial seismic wave and basic combined conditions in the switching 0+062 section. As shown in Table 5, compared with the static long-term working conditions, the maximum decrease of the factor of safety under the design earthquake reaches 50% for sliding mode I and 40% for sliding mode II. The strong earthquake has a significant effect on the stability safety of the slope.

**Table 5.** Factor of safety for the most dangerous sliding surface under design earthquake working conditions.

Section	Working Condition	Sliding Mode I		Sliding Mode II	
		Minimum	Less than 1.05 Cumulative Time (s)	Minimum	Less than 1.05 Cumulative Time (s)
Plant 0+000	Normative spectrum artificial wave	1.138	0	1.533	0
	Wenchuan earthquake wave	0.93	0.08	1.706	0
	Luchan earthquake wave	0.955	0.12	1.504	0
Plant 0+014	Normative spectrum artificial wave	1.02	0.04	1.909	0
	Wenchuan earthquake wave	0.916	0.26	1.726	0
	Luchan earthquake wave	0.956	0.10	1.617	0
Plant 0+028	Normative spectrum artificial wave	1.014	0.04	1.763	0
	Wenchuan earthquake wave	0.893	0.46	2.103	0
	Luchan earthquake wave	0.85	0.28	2.126	0
Plant 0+038	Normative spectrum artificial wave	1.054	0	1.886	0
	Wenchuan earthquake wave	0.883	0.48	2.206	0
	Luchan earthquake wave	0.857	0.16	1.989	0
Plant 0+051	Normative spectrum artificial wave	0.937	0.44	1.804	0
	Wenchuan earthquake wave	0.862	0.52	2.038	0
	Luchan earthquake wave	0.913	0.48	1.766	0
Switching 0+031	Normative spectrum artificial wave	1.203	0	1.198	0
	Wenchuan earthquake wave	1.029	0.06	1.518	0
	Luchan earthquake wave	1.024	0.02	1.227	0
Switching 0+043	Normative spectrum artificial wave	1.11	0	1.271	0
	Wenchuan earthquake wave	1.153	0	1.384	0
	Luchan earthquake wave	1.091	0	1.311	0
Switching 0+062	Normative spectrum artificial wave	0.908	0.52	1.089	0
	Wenchuan earthquake wave	0.887	0.56	1.012	0.06
	Luchan earthquake wave	0.928	0.46	0.987	0.08

Under the action of the design earthquake, the dynamic stability factor of safety of sliding mode II of each calculated section was greater than 1.05 except for the section 0+062 of the switch station, and the cumulative time of the stability factor of safety of the section 0+062 of the switch station less than 1.05 was only 0.8 s, which is less than 0.3 s, and the slope stability factor of safety meets the dynamic stability requirement. It shows that the artificial slopes of the plant and switching station after reinforcement treatment by comprehensive support measures can still maintain slope stability when encountering the design earthquake, and their seismic safety is guaranteed.

Under the action of the design earthquake, the minimum dynamic stability factor of safety of sliding mode I of each calculated section was less than 1.05 except for the section 0+043 of the switching station, and the cumulative time of factor of safety, less than 1.05 exceeded 0.3 s for the section 0+028 of plant, 0+038 of plant, 0+051 of plant, and 0+062 of the switching station. The factor of safety cannot meet the requirements of dynamic stability in sliding mode I of the slope.

The most dangerous slide-fracture surfaces that could not meet the stability requirements in each section are all located within the natural slopes beyond the slope opening line. In contrast, the minimum dynamic stability safety factor of sliding mode I in each calculated profile was greater than 1.05 in the artificial slope below the opening line, which meets the stability requirements. Therefore, the risks of shallow sliding of the natural slopes outside the slope opening line in the shallow surface layer of the crumbly soil layer of the crumbling slope blocks and the sliding instability along the interface between the cover layer and bedrock are high when encountering the design earthquake. This may pose a safety threat to the operating personnel and equipment of the plant and switching station.

## 5. Conclusions

This study presents a slope stability analysis of a large hydropower station under working conditions, as well as when subjected to the Wenchuan earthquake, Lushan earthquake, and a design earthquake using both the rigid body limit equilibrium method and the finite element method. The most unfavorable sliding surface and the factor of safety of the slope under earthquake actions were investigated. The main conclusions are as follows:

- (1) The slope displacement is basically stable and converging, and the maximum displacement of the slope was about 20 mm during the monitoring period. The slope displacement distribution map shows that the slope displacement in the part above 1441 m elevation is obviously larger than that below. The groundwater table changes with seasons and is higher in the rainy season in summer. The permeability of the rock body near the slope is strong and the drainage performance is good. The groundwater table of the slope is low, which is beneficial to the stability of the side slope.
- (2) The minimum factor of safety of slopes calculated by the two stability analysis methods meets the requirements of the stability safety control standard 1.20 for long-term operational conditions. Under the strikes of Wenchuan and Lushan earthquakes, the safety factors under both sliding modes are reduced compared with the static long-term working conditions. The minimum factor of safety for each section under the Wenchuan and Lushan earthquakes meets the requirement of the safety control standard of 1.05 under seismic conditions. Both the Wenchuan and Lushan earthquakes did not cause significant adverse effects on the overall stability of the slope of the Y hydropower station.
- (3) Under the action of a design earthquake, the minimum dynamic factors of safety of sliding mode I in the many calculated sections were less than 1.05, and the accumulated time of each factor of safety less than 1.05 typically exceeding 0.3 s, while the factor of safety of sliding mode I of the slope could not meet the requirements of dynamic stability.
- (4) Under the design earthquake, the most dangerous sliding surfaces that cannot meet the stability requirements in each section are all located in the natural slope area

beyond the slope opening line. The minimum dynamic factor of safety of sliding mode I of each calculated section was greater than 1.05 in the man-made slope below the opening line, which meets the stability requirement. Therefore, the risk of shallow sliding or sliding instability along the interface between the overburden and bedrock of the natural slope outside the slope opening line is high when encountering the design earthquake, which poses a safety threat to the operating personnel and equipment of the plant and switchyard. Effective seismic defense measures should be developed to ensure that the safety of plant and switching station operators and equipment can still be guaranteed in the event of a strong earthquake.

**Author Contributions:** Conceptualization, H.L. and D.Y.; methodology, D.Y.; validation, J.Y. and J.W.; formal analysis, D.Y.; investigation, H.L.; writing—original draft preparation, D.Y.; writing—review and editing, H.L., J.Y. and J.W.; supervision, H.L.; funding acquisition, H.L. All authors have read and agreed to the published version of the manuscript.

**Funding:** This research was funded by the State Key Laboratory of Building Safety and Built Environment Open Foundation (Grant No.BSBE2021-03).

**Data Availability Statement:** The data presented in this study are available on request from the corresponding author.

**Conflicts of Interest:** The authors declare no conflict of interest.

## References

- Zhongxia, Y.; Depeng, L.; Shuaihua, Y. Stability analysis of high fill slope with loess under earthquake and rainfall infiltration. *J. Lanzhou Univ. Technol.* **2022**, *48*, 119–125. (In Chinese)
- Runyun, F. *Stability Analysis of Three-Dimensional Slope under Complex Stress Conditions*; Lanzhou University of Technology: Lanzhou, China, 2013.
- Yufeng, G.; Di, W.; Fei, Z. Current research and prospects of 3D earth slope stability analysis methods. *J. Hohai Univ.* **2015**, *43*, 456–463. (In Chinese)
- Shangyi, Z.; Weimin, S.; Yingren, Z. FEM for analysis of slope stability. *Contente Abstracts* **2001**, *21*, 450–454. (In Chinese)
- Zeyu, Z. *Three-Dimensional Seismic Stability Analysis of High Faced Rockfill Dam Based on Finite Element Sliding Surface Stress Method*; Dalian University of Technology: Dalian, China, 2018.
- Mingwei, G.; Chuanguang, L.; Shuilin, W. Three-dimensional slope stability analysis based on finite element stress. *Chin. J. Rock Mech. Eng.* **2012**, *31*, 122–128. (In Chinese)
- Yongsheng, L.; Shenghong, C. Search of three-dimensional slip surface for slope based on finite element calculation. *Rock Soil Mech.* **2012**, *34*, 1191–1196. (In Chinese)
- Shunchuan, W.; Aibing, J.; Yongtao, G. Numerical simulation analysis on strength reduction for slope of jointed rock masses based on generalized Hoek-Brown failure criterion. *Chin. J. Geotech. Eng.* **2006**, *28*, 1975–1980. (In Chinese)
- Longqiang, H.; Shunchuan, W.; Zhipeng, L. Study of non-proportional strength reduction method based on Hoek-Brown failure criterion. *Rock Soil Mech.* **2016**, *37*, 690–696. (In Chinese)
- Hammah, R.E.; Yacoub, T.E.; Corkum, B.C.; Curran, J.H. The shear strength reduction method for the generalized Hoek-Brown criterion. In Proceedings of the 40th US Symposium on Rock Mechanics Alaska Rocks, Anchorage, AK, USA, 25–29 June 2005.
- Sun, C.W.; Chai, J.R.; Xu, Z.G. Stability charts for rock mass slopes based on the Hoek-Brown strength reduction technique. *Eng. Geol.* **2016**, *214*, 94–106. [[CrossRef](#)]
- Shen, J.Y.; Karakus, M.; Xu, C.S. Chart-based slope stability assessment using the generalized Hoek-Brown criterion. *Int. J. Rock Mech. Min. Sci.* **2013**, *64*, 210–219. [[CrossRef](#)]
- Shaohua, Z.; Yunlong, H.; Wei, S.; Shi, X. Study of seismic safety of back powerhouse rock slope of Yaoheba hydropower station. *Eng. J. Wuhan Univ.* **2015**, *48*, 483–488. (In Chinese)
- Hanlong, L.; Kang, F.; Yufeng, G. Time history analysis method of slope seismic stability. *Rock Soil Mech.* **2003**, *24*, 553–556. (In Chinese)
- Qi, S.W.; Wu, F.Q.; Liu, C.L.; Ding, Y.H. Engineering geology analysis on stability of slope under earthquake. *Chin. J. Rock Mech. Eng.* **2004**, *23*, 2792–2797. (In Chinese)
- Wang, L.M.; Pu, X.W.; Wu, Z.J.; Sun, J.J.; Wang, P.; Chai, S.F. The shaking table test of the instability sliding of loess slope under the coupling effects of earthquake and rainfall. *Chin. J. Rock Mech. Eng.* **2017**, *36*, 3873–3883. (In Chinese)
- Xu, G.X.; Yao, L.K.; Li, Z.H.; Gao, Z.N. Dynamic response of slopes under earthquakes and influence of ground motion parameters. *Chin. J. Geotech. Eng.* **2008**, *30*, 918–923.
- Tang, D.; Li, D.Q.; Zhou, C.B.; Phoon, K.K. Slope stability analysis considering antecedent rainfall process. *Rock Soil Mech.* **2013**, *34*, 3239–3248. (In Chinese)

19. Shuaihua, Y.; Yilei, S. Stability analysis of Multi-Stage high slope with loess under rainfall infiltration. *J. Eng. Geol.* **2018**, *26*, 1648–1656. (In Chinese)
20. Lin, H.Z.; Yu, Y.Z.; Li, G.X.; Peng, J.B. Influence of rainfall characteristics on soil slope failure. *Chin. J. Rock Mech. Eng.* **2009**, *28*, 198–204. (In Chinese)
21. Lee, W.F.; Liao, H.J.; Chen, R.H.; Wei, C.Y.; Huang, Y.M. The Development and Application of the Slope Management System. *GeoCongress 2006, 2006*, 1–6.
22. Fredlund, D.G. Slope stability hazard management systems. *J. Zhejiang Univ. Sci. A* **2007**, *8*, 1695–1711. [[CrossRef](#)]
23. Hack, R.; Alkema, D.; Kruse, G.A.M.; Leenders, N.; Luzi, L. Influence of earthquakes on the stability of slopes. *Eng. Geol.* **2007**, *91*, 4–15. [[CrossRef](#)]
24. Liu, Y.; Li, H.; Xiao, K.; Li, J.; Xia, X.; Liu, B. Seismic stability analysis of a layered rock slope. *Comput. Geotech.* **2014**, *55*, 474–481. [[CrossRef](#)]
25. Zhou, X.P.; Cheng, H. Stability analysis of three-dimensional seismic landslides using the rigorous limit equilibrium method. *Eng. Geol.* **2014**, *174*, 87–102. [[CrossRef](#)]
26. Ceryan, N.; Kesimal, A.; Ceryan, S. Chapter 13—Probabilistic Analysis Applied to Rock Slope Stability: A Case Study from Northeast Turkey. In *Integrating Disaster Science and Management*; Samui, P., Kim, D., Ghosh, C., Eds.; Elsevier: Amsterdam, The Netherlands, 2018; pp. 221–261.
27. Jelínek, J.; Žáček, V. Assessment of a catastrophic rock avalanche in the West Mongolian Altai Mountains. *Eng. Geol.* **2018**, *233*, 38–47. [[CrossRef](#)]
28. Doi, I.; Kamai, T. Relationship between earthquake-induced excess pore water pressure and strong ground motion observed in a monitored fill slope. *Eng. Geol.* **2020**, *266*, 105391. [[CrossRef](#)]
29. He, J.; Qi, S.; Wang, Y.; Saroglou, C. Seismic response of the Lengzhuguan slope caused by topographic and geological effects. *Eng. Geol.* **2020**, *265*, 105431. [[CrossRef](#)]
30. Bao, Y.; Huang, Y.; Zhu, C. Effects of near-fault ground motions on dynamic response of slopes based on shaking table model tests. *Soil Dyn. Earthq. Eng.* **2021**, *149*, 106869. [[CrossRef](#)]
31. Wu, Z. *Stability and Risk Analysis of Powerhouse Slope of Nanya River Yaoheba Hydroelectric Station*; Sichuan University: Chengdu, China, 2006.
32. *China Ministry of Water Resources of the People's Republic of Design Specification for Slopes in Water and Hydropower Projects*; China Water Power Press: Beijing, China, 2007.
33. (Ndr) National Development and Reform Commission. *Design Specification for Slope of Hydropower and Water Conservancy Project*; Northwest Survey and Design Institute of China Hydropower Consulting Group: Beijing, China, 2006.
34. *China Ministry of Water Resources of the People's Republic of Specificatins for Seismic Design of Hydraulic Structures*; China Research Institute of Water Resources and Hydropower: Beijing, China, 1997.

**Disclaimer/Publisher's Note:** The statements, opinions and data contained in all publications are solely those of the individual author(s) and contributor(s) and not of MDPI and/or the editor(s). MDPI and/or the editor(s) disclaim responsibility for any injury to people or property resulting from any ideas, methods, instructions or products referred to in the content.